A First Sample of Dust Attenuation Laws for DES Galaxies

João Duarte*
CENTRA, Departamento de Física,
Instituto Superior Técnico, Universidade de Lisboa

Supervisors: Ana Mourão and Santiago González Gaitán
CENTRA, Departamento de Física,
Instituto Superior Técnico, Universidade de Lisboa
(Dated: October 30, 2021)

Type Ia supernovae (SNe Ia) are useful distance indicators in cosmology, provided their luminosity has been calibrated by applying some corrections. One of the factors motivating these corrections is dust extinction, accounted for in the β color-luminosity relation of the calibration. We propose an alternative approach to infer dust attenuation laws towards the host galaxies of 162 SNe Ia, from both global and local (4 kpc) photometry. Simple Stellar Population models are fitted to optical photometry obtained from the Dark Energy Survey, complemented when possible with GALEX UV and 2MASS NIR photometry. We show 4 filters bands are sufficient to recover dust properties for hosts consistently with literature predictions based on both simulations and observations.We show dust properties vary greatly across different galaxies, meaning an universal SN Ia correction cannot be assumed. We find a relation between the attenuation slope and the optical depth, both locally and globally, best explained by varying star/dust geometry with galaxy orientation. This relation is shown to be very different from the extinction found directly for SNe. Analyzing the Hubble residuals for the SNe, we find optical depth and attenuation slope related steps, interpreted as less significant reflections of the "mass-step". An entirely dust motivated description of this phenomenon is found to be possible when employing a two dimensional "dust-step". We study a new SNe Ia calibration, separating the intrinsic and extinction contributions in the color-luminosity correction, the latter being approximated by host attenuation. We conclude it is worse than the standard calibration.

Keywords: supernovae calibration; dust extinction; dust attenuation; distance scale

I. INTRODUCTION

Type Ia supernovae (SNe Ia) are cosmological objects that make for excellent distance indicators, having famously contributed to the discovery of the accelerated expansion of the Universe[1][2]. This is because their luminosity can be standardized by applying some empirical corrections based on color-luminosity and light curve shape-luminosity relations[3]. A third correction is often introduced, as there is evidence for a luminosity dependence related to the stellar mass of the SN Ia host galaxy $M_\star$ [4], even after the application of the other corrections.

These corrections are used to estimate the absolute magnitude of a SN Ia, from which the luminosity distance d_L to the SN can be obtained by comparison with the observed apparent magnitude. This distance is often indirectly parameterized by means of the distance modulus μ, defined as the difference between the apparent and absolute magnitudes of a given celestial object:

$$\mu = 5\mathrm{Log}\left(\frac{d_L}{10\mathrm{pc}}\right) \tag{1}$$

The standardization of a group of SNe Ia begins with a fit of the light-curve for each SN, returning values for the light-curve width x_1, colour c, and observed magnitude m_B. One can then perform a fit to convert the light curve fit parameters into corrected distance modulus values μ and to determine nuisance parameters α, β, γ and M. These parameters describe the shape-luminosity, color-luminosity and mass step corrections, as well as the absolute magnitude of a fiducial SN Ia with $x_1 = 0$ and $c = 0$. The corrected distance modulus μ for each SN Ia is given by[3]:

$$\mu = m_B - M + \alpha x_1 - \beta c + \delta_M, \tag{2}$$

where δ_M is the "mass step" term, which is dependent on the host galaxy mass and γ[5]:

$$\delta_M = \begin{cases} \frac{\gamma}{2}, & \text{if } \mathrm{Log}(M_\star/M_\odot) > 10 \\ -\frac{\gamma}{2}, & \text{if } \mathrm{Log}(M_\star/M_\odot) < 10 \end{cases}. \tag{3}$$

For each SN, the deviation between the value obtained for μ from Eq. 2 and the expected distance modulus μ_{model} in a given cosmological model is known as an Hubble residual $\Delta\mu = \mu - \mu_{\mathrm{model}}$.

As expressed in Eq. 1, μ_{model} is simply a function of the luminosity distance d_L which, for a Friedmann-Robertson-Walker cosmology, only depends on the cosmological parameters and the redshift[1]. In this work, we assume a spatially-flat ΛCDM model[6], with a matter density $\Omega_m = 0.3$, a dark energy density of $\Omega_\Lambda = 0.7$ and an Hubble constant $H_0 = 70\mathrm{km\,s^{-1}\,Mpc^{-1}}$. Under these assumptions, the luminosity distance is given by[5]:

* Supported by CRISP Project (PTDC/FIS-AST-31546/2017)

$$d_L(z) = (1+z)c\int_0^z \frac{dz'}{H_0\sqrt{\Omega_m(1+z')^3+\Omega_\Lambda}} \quad (4)$$

Two main factors contribute to the β color-luminosity correction in Eq. 2: the intrinsic color variations among different SNe Ia and the effects of astrophysical dust, in particular reddening. These effects can be described by one of two distinct concepts: extinction or attenuation, depending on whether we are dealing with a point, such as a SN Ia, or extended source, respectively[7].

Extinction results from the overall composition, size and orientation of the dust grains. It refers to the absorption of light as well as scattering of that light out of the line of sight. Both of these effects tend to be stronger for blue light, as its wavelength is comparable to the typical size of dust grains (5 to 250 nm)[7]. This leads to a dimming and reddening of the observed spectrum.

Attenuation includes not only the above mentioned effects, but also effects arising from the spacial distribution of stars and dust in a galaxy or stellar population, such as scattering of light back into the line of sight, variable dust densities and light emitted by unobscured stars. Attenuation is discussed in the context of galaxies and other extended objects, as the previously described phenomena are negligible when considering only a single star.

Three quantities are important when describing extinction/attenuation: the extinction/attenuation for the V band A_V, which is roughly equal to the optical depth of the dust for this band τ_V; the color excess $E(B-V)$; and the ratio of total-to-selective extinction R_V, which describes the level of reddening:

$$E(B-V) = A_B - A_V \quad (5)$$

$$R_V = \frac{A_V}{E(B-V)}, \quad (6)$$

where $\lambda_V = 5510$Å and $\lambda_B = 4450$Å. More generally, the extinction/attenuation at a given wavelength λ, $A(\lambda)$, is usually parameterized by a curve $k(\lambda)$:

$$A(\lambda) = \frac{A_V}{R_V}k(\lambda) \iff \tau(\lambda) = \frac{\tau_V}{R_V}k(\lambda). \quad (7)$$

If the existence of the β color-luminosity relation in Eq. (2) was entirely due to dust, then we would have[8]:

$$\beta_{R_V} = R_V + 1 \quad (8)$$

For the purposes of standardization, the value of β is assumed to be the same for the entire population of SNe Ia under study. However, it has been shown that dust properties can vary between galaxies[7][9], and so assuming a common β for all SNe may negatively impact the Hubble residuals. It can thus prove advantageous to individually determine dust properties for each SN Ia.

In this work we present an alternative approach to infer dust attenuation laws towards the host galaxies for a cosmological sample of 162 SNe Ia collected as part of the Dark Enery Survey (DES)[10][11].

To achieve this goal, we use photometric data in the *griz* filter bands for the SNe hosts. We fit Simple Stellar Population (SSP) models to this data, from which we extract relevant information about the dust properties for each individual galaxy.

Furthermore, we study the relation between a host galaxy's attenuation law and its respective SN extinction law, analysing the viability of using our fit results to approximate the latter. In particular, we are interested in the impact of using the values of R_V, inferred for the host galaxies, in a new SNe Ia calibration.

Finally, we explore possible origins of the "mass-step" relation, analysing whether it can be linked to or described by the attenuation law of the SNe host galaxies.

II. DATA AND METHODS

A. Dark Energy Survey Photometric Data

The Dark Energy Survey (DES) is an imaging survey covering ~ 5100 square degrees of the southern hemisphere using the 4-m Blanco telescope at the Cerro Tololo Inter-American Observatory (CTIO), equipped with the 520 megapixel wide-field Dark Energy Camera [12] with a 0.263 arcsecond/pixel resolution.

In this work we look at data collected as a part of the first three-year cosmological sample of the survey (DES3YR)[1][5], consisting of 162 spectroscopically-confirmed SNe Ia, as well as their respective host galaxies[13][14]. This data covers a redshift range of $0.077 < z < 0.58$ and includes both global and local broadband photometry for the hosts in the DECam *griz* filter bands, originally computed by Kelsey (2020)[11].

The global photometry for each host galaxy was measured from stacked images using **SOURCE EXTRACTOR**[15], employing Kron FLUX_AUTO measurements. A detection image was used to set the aperture, which ensures the aperture is the same for the measurements in each filter. The measurements were also corrected for Milky Way dust extinction using Schlegel dust maps[16] and a Fitzpatrick extinction law[17] with coefficients $R_g = 3.186$, $R_r = 2.140$, $R_i = 1.569$ and $R_z = 1.196$[11].

In the case of local photometry, the aperture photometry tool from the **PHOTUTILS** Python module [18] was used. The resulting fluxes were corrected for Milky Way extinction in the same way as described above[11].

[1] `https://www.darkenergysurvey.org/des-year-3-supernova-cosmology-results/`

A maximum threshold FWHM of 1.3″ was assumed for the seeing[11]. Thus, assuming a Gaussian form for the point spread function (PSF) with FWHM $= 2\sqrt{2\ln(2)}\sigma$, we obtain a smallest useful aperture radius of $\sigma = 0.55''$. Given that a 4 kpc aperture only becomes smaller than a $0.55''$ radius near $z \simeq 0.7$[11], we can choose a consistent 4 kpc radius aperture for our analysis.

B. Bayesian Inference

We are interested in fitting Simple Stellar Population (SSP) models to our photometric data. We do this by computing the Spectral Energy Distributions (SED) for each SSP and comparing with the observed data. We rely on Bayesian inference methods to do so, using the **Prospector**[2][19] and **emcee**[3][20] Python packages.

We start by assuming that a given data set D_{obs}, comprised of N points, can be modeled using a probability distribution function (pdf) $p(D|\boldsymbol{\theta})$. This is known as the likelihood and it is a function of a parameter vector $\boldsymbol{\theta}$:

$$\mathcal{L}(\boldsymbol{\theta}) = p(D_{obs}|\boldsymbol{\theta}) \tag{9}$$

One common definition for $\mathcal{L}(\boldsymbol{\theta})$ is given by:

$$\mathrm{Ln}(\mathcal{L}(\boldsymbol{\theta})) = -\frac{1}{2}\sum_{i=0}^{N}\left(\frac{\Delta(\boldsymbol{\theta})_i^2}{\sigma_i^2} + \ln(2\pi\sigma_i^2)\right), \tag{10}$$

where $\Delta(\boldsymbol{\theta})$ is the difference between the observations and the fitted model and σ^2 accounts for observation errors.

To describe the parameters $\boldsymbol{\theta}$, we define a set of pdf's $p(\boldsymbol{\theta})$ known as priors, which essentially describe the information we have about $\boldsymbol{\theta}$ before looking at the data. Inference can therefore be thought of as a process of updating the prior based on observed data. We call this updated pdf $p(\boldsymbol{\theta}|D_{obs})$ the posterior and it can be obtained from the application of Bayes' Theorem:

$$p(\boldsymbol{\theta}|D_{obs}) = \frac{p(D_{obs}|\boldsymbol{\theta})p(\boldsymbol{\theta})}{p(D_{obs})}, \tag{11}$$

where $p(D_{obs})$ is known as the predictive prior and acts simply as a normalization constant. It can also be helpful to define a single *best-fit* value for a parameter. We take this value to be the median of the posterior, with the 16th and 84th percentiles defining a 68% credible region.

To mitigate some of the computational drawbacks of Bayesian inference, we use a method know as sampling, which allows one to reconstruct the posterior based on a set of discrete values for $\boldsymbol{\theta}$. As such, a computation over the entire parameter space is no longer necessary.

In this work, we use the Metropolis–Hastings Markov Chain Monte Carlo (M-H MCMC) sampling algorithm[21]. This algorithm produces a biased random walk through parameter space, which will tend to converge towards values of $\boldsymbol{\theta}$ that maximize the posterior pdf. We will thus end up with a discrete set of values of $\boldsymbol{\theta}$, known as a walker, from which we can then obtain a fairly close reconstruction of the posterior.

Some steps can be taken to improve on this algorithm. Increasing the number of walkers used mitigates the pitfall of local maxima in the posterior, in which some of the walkers might get stuck. As the initial iterations of each walker depend highly on the initial values of the algorithm, it is also common to perform a number of initial samplings whose values are discarded to eliminate any bias. This is known as the burn-in.

One can also improve on the choice of initial values $\boldsymbol{\theta}_0$ by performing a set of initial minimizations on the data, which provide useful insights about the region where the walkers should be initialized. However, not all walkers should be initiated on the exact result of the initial minimization. Rather, each walker should be initiated within a certain radius around the minimization results. This radius is known as the initial dispersion D_θ.

After extensive testing, we settled on the following configuration for the sampling algorithm:

- 20 initial minimizations;
- 128 walkers;
- 3 initial rounds of burn-in, with 16, 32 and 64 iterations, respectively;
- 1024 iterations for each walker (after burn-in).

C. SSP Models

For the models used to calculate $\Delta(\boldsymbol{\theta})$ in Eq. 10, we use SSP models, which assume that all stars in the considered population were born at the same time from a cloud of homogeneous chemical composition[22]. In particular, we loosely follow the PROSPECTOR-α model[19], referring to the Padova isochrones[23] to build the model. The models were generated using the **FSPS**[4][24][25] FORTRAN code and the **python-FSPS**[5] Python package.

There are some important concepts to consider when building a SSP model, namely: stellar mass $M_\star$; star formation history (SFH); stellar metallicity $Z_\star$; dust attenuation; and redshift z.

The main contribution of the total stellar mass of the galaxy to the SED is to set the overall normalization. The distribution of this stellar mass $M_\star$ in a galaxy can be described by an empirical initial mass function (IMF),

[2] `https://github.com/bd-j/prospector`
[3] `https://github.com/dfm/emcee`
[4] `https://github.com/cconroy20/fsps`
[5] `https://github.com/dfm/python-fsps`

from which the present day mass distribution can be obtained by simulating the evolution of the population. In this model, we use a Kroupa (2001) IMF[26].

The stellar mass is fairly easy to constrain based on observed data, even while other parameters might exhibit some degeneracy among themselves. For this reason, and given that the available photometric data is insufficient for a more complete fit, we will treat the stellar mass as a fixed parameter. In particular, we will use previously obtained values for these masses.

The star formation history (SFH) describes how stars form over time and space in a galaxy. This is relevant to the SED, as young stellar populations tend to exhibit a bluer spectrum, as massive and short-lived stars dominate the emission, while older populations exhibit a redder spectrum, since the more massive stars have died out and the low mass stars are reaching the end stages of their evolution [27]. In this work, we adopt a delayed τ-model, with the SFH described by an exponentially decreasing star formation rate (SFR), with e-folding time τ:

$$SFR(t) = te^{-t/\tau}, \tag{12}$$

where t is the time measured from the beginning of the Universe up to the age of the stellar population $t_{\rm age}$.

We treat the SFH parameter as a fixed value, with $\tau =$ 1Gyr. Contrastingly, the age parameter $t_{\rm age}$ is always left free. For this parameter, we choose a flat top-hat prior over the range $0.001 < t_{\rm age} < 13.8$ Gyr. Additionally, we choose $D_{t_{\rm age}} = 5$ Gyr for the initial age dispersion.

Stellar metallicity Z is defined as the abundance of elements heavier than helium in a star. It mainly affects the optical to near-infrared (NIR) flux ratio, which is important when determining dust attenuation. Metallicity is thus always introduced as a free parameter in our model.

We choose a flat top-hat prior on the logarithm of the metallicity over the range $-2 < \mathrm{Log}(Z_\star/Z_\odot) < 2.5$. This range is mostly determined by the coverage of the Padova isochrones[23], which covers $-2 < \mathrm{Log}(Z_\star/Z_\odot) < 0.2$. Nevertheless, we extend the upper limit in our prior to assure a more complete sampling of the parameter space. Additionally, we choose $D_{\mathrm{Log}(Z_\star/Z_\odot)} = 2$.

The impacts of dust attenuation on a SED and its parametrization have already been discussed. In our model we will be referring to a modified version of the attenuation curve derived by Calzetti[28]. The original curve $k(\lambda)$ follows Eq. 7 and has an original total-to-selective attenuation of $R_{V,0} = 4,05$.

Observations show that this curve can be insufficient to describe attenuation processes for star-forming galaxies, in particular at higher redshifts. In these cases there is evidence of a UV bump at ~ 2175Å[29]. For this reason, the original curve is modified by the addition of this same bump, modelled by a Lorentzianlike "Drude" profile:

$$D(\lambda) = \frac{E_{bump}\lambda^2\gamma^2}{(\lambda^2 - \lambda_0^2)^2 + \lambda^2\gamma^2}, \tag{13}$$

where $\lambda_0 = 2175$Å is the central wavelength, $\gamma = 350$Å is the FWHM of the bump and E_{bump} is the amplitude[29]. We will further discuss this amplitude shortly.

Additionally, the modified attenuation law is also multiplied by a power law $\left(\frac{\lambda}{\lambda_V}\right)^n$ in order to produce different slopes without the need to alter τ_V. The slope, and thus the reddening, ends up being effectively controlled by the dust attenuation index n[29].

There is evidence of a relation between the steepness of the attenuation curves and the strength of the UV bump[30]. This means that E_{bump} exhibits a dependency in n, which, can be described by $E_{bump} = 0.85 - 1.9n$.

Taking these corrections into account, the moddified Calzetii attenuation law becomes[29]:

$$\tau(\lambda) = \frac{\tau_V}{R_{V,0}}[k(\lambda) + D(\lambda, n)]\left(\frac{\lambda}{\lambda_V}\right)^n. \tag{14}$$

The dust attenuation for this model is parametrized by Eq. (14), with τ_V and n acting as free parameters.

In the case of τ_V, we adopt a flat top-hat prior over the range $0 < \tau_V < 6$ to account for a fairly large range of optical depths. Additionally, we choose $D_{\tau_V} = 1$.

In the case of n, we also adopt a flat top-hat prior, this time over the range $-2.2 < n < 0.4$ to account for the typical slopes in attenuation curves. The upper limit is chosen so that we do not end up with a flat attenuation curve, which would cause $\tau(\lambda)$ to be nearly fully degenerate with the normalization of the SED[19]. For the initial dispersion in n, we choose $D_n = 1$.

Finally, the redshift z must be accounted for in our model, in order to make sure the effects of the expansion of the Universe are represented in the SED. For each SN host, the redshift is treated as a fixed parameter, as the DES galaxies have spectroscopically confirmed redshifts[11][13].

III. TEST SIMULATIONS

We begin by performing some tests to see how accurately the fitting method can recover the model parameters from broadband photometric data. We do this by performing fits on a simulated galaxy population.

The first step of the test is to simulate galaxy SEDs from which to extract the relevant photometric data. We do this by once again using **FSPS**, employing the same SSP model as described in the previous section, with the values for $M_\star$, $Z_\star$, $t_{\rm age}$, τ_V, n, and z being drawn from a series of statistical distributions. According to this process, a population of 75 mock galaxies was generated.

From the resulting models, SEDs for each galaxy were generated. These were then used to extract broadband photometry in the DECam *griz* filter bands[6][13][14]. Additionally, a degree of Gaussian noise was applied to the

[6] http://www.ctio.noao.edu/noao/node/13140

data in accordance with a prescribed signal-to-noise ratio (SNR) of 10. This value was chosen to roughly reflect the minimum SNR of the DES data set[11].

For each galaxy we have 4 data points and are therefore limited to 4 free fit parameters. For this reason, both the redshift and the stellar mass for the galaxies were treated as fixed parameters, as previously discussed. Both of these values are therefore set to the values used to generated the simulated photometry.

Regarding the fit results, we find, in comparison with the "true" simulation values, a median bias of 0.094 and a $RMS = 0.952$ for τ_V and a median bias of -0.024 and a $RMS = 0.364$ for n.

Some subsequent tests were performed using additional GALEX UV and 2MASS NIR photometry. While some cases showed marginal improvement, it is overall reasonably to conclude that optical photometry is sufficient to accurately determine dust properties for galaxies.

IV. DUST ATTENUATION FOR DES GALAXIES

Having tested the proposed fitting method, we now move on to the fits for both the global and local DES photometric data. Once again, we treat the stellar mass as a fixed parameter, referring to the values previously obtained for these galaxies by Kelsey (2020)[11].

We begin by examining the correlation between the *best-fit* values for the attenuation parameters, τ_V and n, plotted in Fig.1. A Gaussian Process Regression and respective 68% credible interval, performed using the **GauPro**[7][31] R package, is also plotted to better illustrate the observed correlation. For comparison, the mean relation obtained by Chevallard (2013)[32] for the overall correlation between these two quantities for a set of simulated galaxies observed at different angles is also shown.

Despite some scatter, there is a clear correlation between the two quantities in both the global and local cases, with larger optical depths corresponding to larger values of n, and thus shallower attenuation curves. It should be noted, that the fitted curves are not representative of the data for $\tau_V > 2.5$.

Although the Chevallard model simulation relation differs slightly from our data we can see that it expresses the same overall tendency. We are thus fairly confident that the overall correlation between the two dust parameters can be explained by different galaxy orientations.

The cases with small τ_V, mostly correspond to galaxies that are being observed face-on. To understand the important phenomena governing observations in this case, we must consider both the photons emitted parallel and perpendicularly to the galaxy plane.

Photons emitted perpendicularly to the galaxy plane, that is, along the line of sight for a face-on galaxy, suffer minimal attenuation, independently of their wavelength. Additionally, we must also take into account photons emitted along the equatorial plane of a galaxy, which might be scattered away from the plane and into the line of sight. On one hand, for blue photons, which interact strongly with the dust particles, the probability of escaping the plane in this manner is low, as they are likely to continue interacting with the dust particles even after being scattered, eventually being fully absorbed[32]. On the other hand, red photons, which do not interact as strongly with dust particles, have a higher change of not meaningfully interacting with dust after this scatter event, which allows them to more consistently escape the galaxy plane in this fashion. This leads to higher values of reddening, reflected in more negative values for n.

The cases with a larger τ_V correspond to a edge-on view of the galaxies. In these cases, radiation emitted from the deepest layers of the galaxy is fully absorbed, independently of wavelength. The radiation reaching an observer is thus dominated by stars located in the outermost layers of the galaxy, unobscured stars and light scattered into the line of sight[33]. This leads to an overall lower level of reddening and values of n closer to 0.

It should be noted that galaxy orientation is not the only mechanism behind the correlation observed in Fig. 1, being mostly relevant for spiral galaxies. For elliptical galaxies, for example, galaxy orientation is not an important factor. However, due to the overall low dust content for these particular galaxies, they end up exhibiting a behaviour similar to the one observed for head-on spiral galaxies, leading to an overall large level of reddening. Additionally, different galaxies can have different intrinsic optical depths, which is one of the possible reasons for the scatter observed in the figure.

Another relevant question is the way the fit parameters relate to the stellar mass, particularly the dust parameters. The *best-fit* dust parameters for each galaxy are thus plotted as a function of stellar mass in Fig. 2.

Despite some scatter, we can see that τ_V increases steadily with $\mathrm{Log}(M_\star/M_\odot)$ for both the global and local cases, up to $\mathrm{Log}(M_\star/M_\odot) \simeq 10$. This tendency is in agreement with results obtained for star-forming galaxies by Salim (2018)[9]. This data, however, describe a continuous increase in τ_V even after the $\mathrm{Log}(M_\star/M_\odot) \simeq 10$ limit, which does not match our results. The large scatter observed for higher stellar masses points to the fact that our data set includes not only star-forming galaxies, but also quiescent galaxies, which typically have lower optical depths and steeper attenuation slopes[9].

Looking now at n, it is clear that this quantity exhibits a behaviour similar to that of the optical depth which, given the strong correlation shown between the two quantities, is not very surprising. As mentioned before, quiescent galaxies tend to have steeper attenuation curves slopes, which is probably the reason for the comparatively more negative values of n found for higher masses.

As previously discussed, observation orientation is one of the main mechanisms governing galaxy attenuation

[7] `https://github.com/CollinErickson/GauPro`

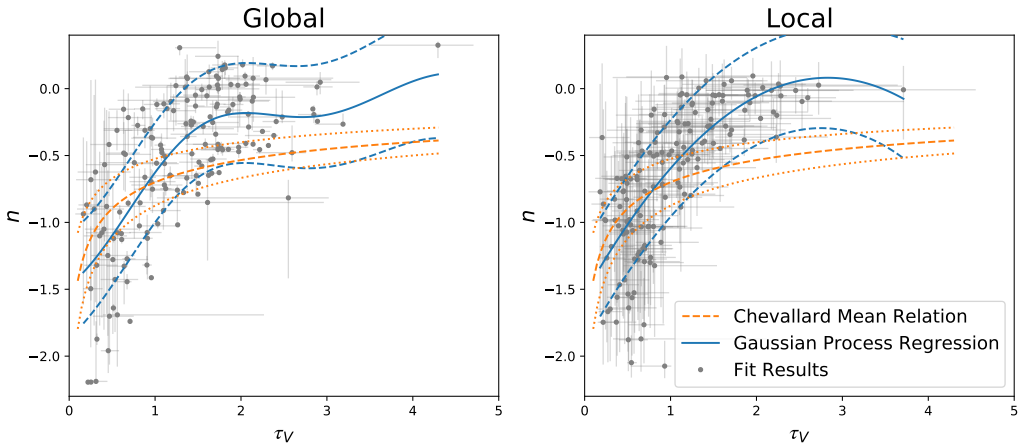

FIG. 1. *Best-fit* values of n as a function of τ_V for the fitted DES galaxies with DECam global (Left panel) and local (Right panel) *griz* photometry. Results for the different galaxies are shown in grey. A Gaussian Process Regression is shown in solid blue, with dashed blue lines defining a 68% credible interval. The mean relation found for similar galaxies by Chevallard (2013)[32] is shown in dashed orange, with ±25% error margins shown in dotted orange.

law. This is one possible explanation for the large scatter observed in Fig. 2. This is one of the reasons why it is important to look at the median values in each bin, so as to get a fair representation of the real physical tendencies across different galaxy orientations.

Overall, despite some level of scatter, the two sets of fits give rise to similar results, which are also in agreement with literature predictions and observations, at least on a general level. Comparing both fits, we find median biases $\Delta\tau_V = 0.26$ and $\Delta n = 0.026$. Even so, it should be noted that the results obtained for τ_V tend to be larger for the global photometry fit.

V. DUST EXTINCTION FOR SNE IA

As previously discussed, the phenomena governing dust extinction differ from those governing attenuation, as the geometrical effects related to the spacial distribution of dust and light sources cease to be relevant, and only the amount and type of dust is important.

To examine the way dust effects differ between point sources (SNe Ia) and extended objects (host galaxies), we plot in Fig. 3 the *best-fit* values for R_V and τ_V for the DES host galaxies. The values of R_V can be easily obtained from Eqs. 6 and 14. As a term of comparison, we look at the correlation found by Mandel (2011)[34] between R_V and τ_V for a set of SNe Ia extinction.

Despite the large error margins for each of the fits, it is clear that the extinction for SN Ia and the attenuation for host galaxies exhibit two opposite tendencies.

The rationale for the correlation found for the parameters in the galaxies' attenuation laws has already been discussed in detail. In summary, it is a combination of effects stemming from both star to dust geometry and galaxy observation orientation.

For a point source, however, these effects are not relevant, and thus we end up with lower values of reddening, an thus higher R_V, for lower optical depths. This happens because photons don't have that many opportunities to interact with dust grains, ending up with fairly uniform extinction for different wavelengths.

As the optical depth increases so do the interaction opportunities, and thus we see a decrease of R_V with τ_V, as the level of reddening grows. Once again, the factors governing galaxy dust attenuation are no longer relevant.

It is also worth noting that the fit results obtained are consistent between global and local observations, which indicates that an aperture of 4kpc is not sufficiently small to negate the geometrical effects associated with attenuation, meaning one needs even smaller physical apertures to correctly account for dust extinction.

These results show that there is not an exact one-to-one relation between SN extinction and host galaxy attenuation, which might introduce problems if the latter is used to extrapolate new β values for a SNe Ia calibration.

VI. SNE IA COSMOLOGY

We will now look at SNe Ia calibration, considering its effects on the Hubble residual. In particular, we will examine two questions: whether there is evidence for a dust related "step" in the data and how it compares to the more commonly used "mass-step"; and what are the effects of using both the global and local individual R_V values obtained for the host galaxies' in a new SNe Ia calibration. We are particularly interested in whether the "mass-step" observed for the Hubble residuals might in fact prove to be an artifact of the universal β calibration.

We will thus look at two different calibrations. The first follows the standard Eq. 2, with an universal fitted

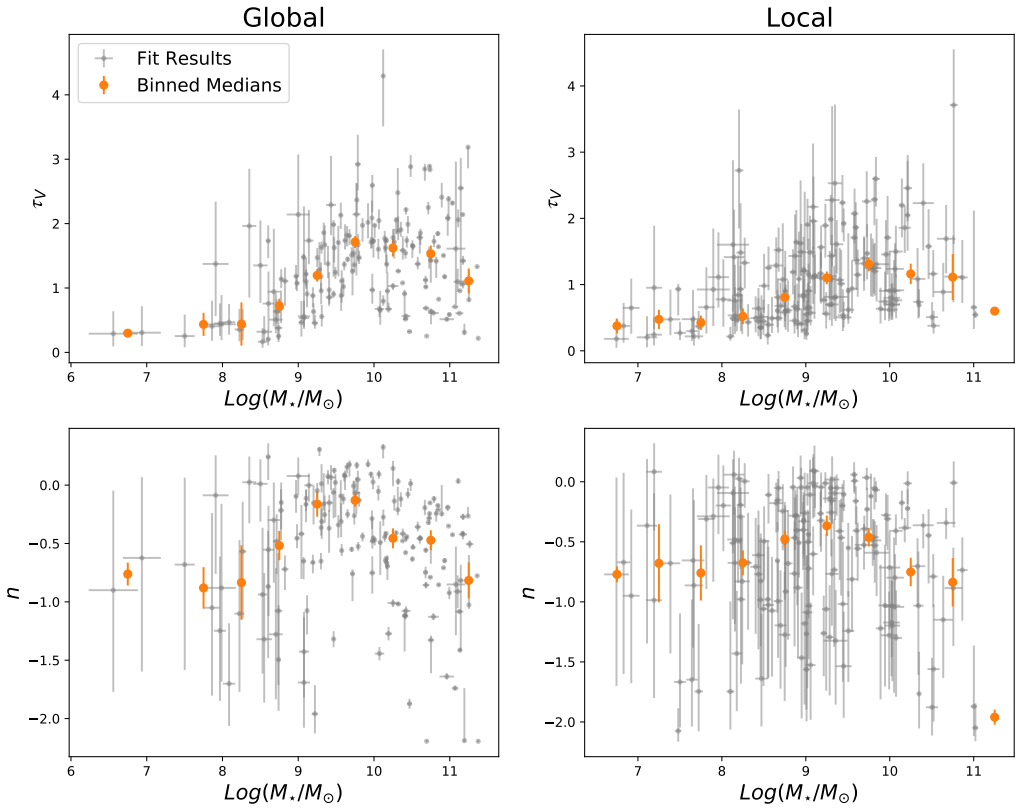

FIG. 2. *Best-fit* results for the dust parameters as a function of $\mathrm{Log}(M_\star/M_\odot)$ for the fitted DES galaxies with DECam global (Left panels) and local (Right panels)*griz* photometry. Plots for τ_V are shown in the top row, while results for n are shown in the bottom row. Results for the different galaxies are shown in grey. Binned medians for each parameter are shown in orange.

β. In this particular case, we set $\delta_M = 0$, so as to make the calibration specific contributions to the "mass-step" more apparent. For the second calibration, we take advantage of the previously obtained values of R_V for the SNe host galaxies to model SNe Ia extinction. Using Eq. 8, we can separate the extinction β_{R_V} and intrinsic β_{int} components in the β color-luminosity relation in Eq. 2. Thus, for this new calibration, we have[35]:

$$\beta c = \beta_{R_V} E(B-V) + \beta_{\mathrm{int}}(c - E(B-V)), \qquad (15)$$

where R_V and $E(B-V)$ are, in this case, the attenuation parameters obtained for both the global and local cases. We once again use a Bayesian fitting procedure for the calibrations, with overall flat priors for the parameters.

A. Standard SNe Ia Calibration

For the standard calibration, the *best-fit* values found were $\alpha = 0.150^{+0.012}_{-0.010}$, $\beta = 3.157^{+0.011}_{-0.009}$ and $M = -19.372^{+0.010}_{-0.007}$. These values result in a fit $RMS = 0.137$.

To look for a "mass-step", we begin by dividing the Hubble residuals into two populations, according to the stellar mass of the respective host galaxy. By varying the value at which the division is made, we can determine the optimal mass value for the step. This can be done by looking at several different quantities.

To begin with, we can look at the step magnitude found at each location, which is defined as the difference between the mean values of the Hubble residuals on each side of the step. This quantity is not very informative by itself, as we must take its error margin into account, which is done by looking at the step significance in σ. Finally, we can look at how much the introduction of the step benefits the overall description of the behaviour of the Hubble residuals. We do this by analysing the difference between the RMS_{mean} for a single population mean description and the RMS_{step} for a dual population mean description with a "mass-step". Thus, the larger the value of ΔRMS, the better a particular step locations is at reducing the Hubble residuals.

The results for the step magnitude, significance and ΔRMS found for the respective Hubble residuals are

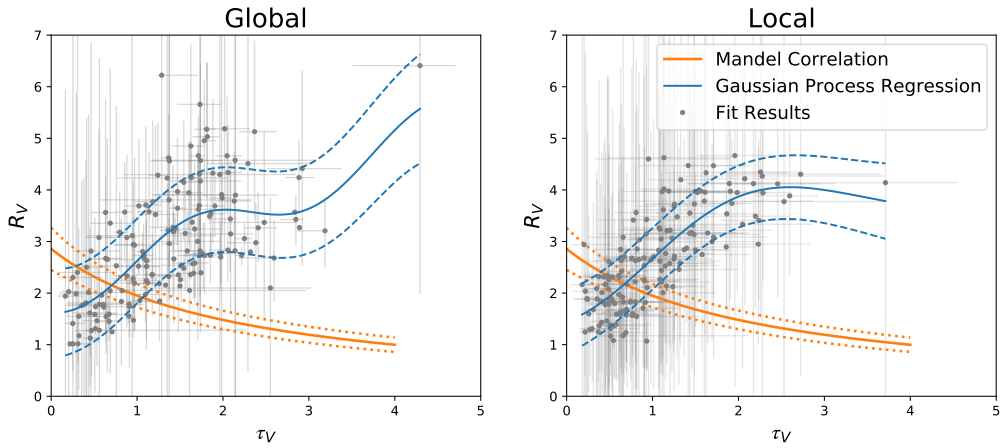

FIG. 3. *Best-fit* values of R_V as a function of τ_V for the fitted DES galaxies with DECam Global (Left panel) and Local (Right panel) *griz* photometry. Results for the different galaxies are shown in grey. A Gaussian Process Regression is shown in solid blue, with dashed blue lines defining a 68% credible interval. The correlation found by Mandel (2011)[34] between these two quantities for the extinction laws of a set of SN Ia is shown in orange.

plotted in Fig. 4. In the case of global measurements, the optimal step location is found to be at $\mathrm{Log}(M_\star/M_\odot) = 9.77$, with a maximum significance of 4.02σ, a step magnitude of 0.080 ± 0.020 mag and $\Delta RMS = 0.0060$. In the local case, the optimal step location is found to be at $\mathrm{Log}(M_\star/M_\odot) = 9.405$, with a maximum significance of 5.35σ, a step magnitude of 0.115 ± 0.022 mag and $\Delta RMS = 0.0115$. Not only are both optimal steps significant at $> 4\sigma$, but they also correspond to the best improvement in RMS. Both step locations and their respective significance levels also roughly match the results obtained by Kelsey (2020)[11] for this data set. This is very solid evidence for the existence of the "mass-step".

With the presence of the "mass-step" established, we will next look at whether evidence for a step related to the dust content of a SN host can be found in the data. In particular, we will examine a possible "τ_V-step", related to τ_V, and an "n-step", related to n.

Following a similar procedure for the "τ_V-step", we find the global optimal step location to be $\tau_V = 2.145$, with a maximum significance of 3.27σ, a magnitude of 0.104 ± 0.032 mag and $\Delta RMS = 0.0033$. In the local case, we find the optimal step location to be $\tau_V = 1.29$, with a maximum significance of 3.40σ, a step magnitude of 0.083 ± 0.024 mag and $\Delta RMS = 0.0050$. These significance levels are lower than those of the "mass-step", but the measured steps are still significant at $> 3\sigma$.

It should be mentioned that, in the global case, there is a slightly less significant candidate for the optimal step location at $\tau_V = 1.78$. For this step location we have $\Delta RMS = 0.0040$, making it more meaningful than the the maximum significance location, as it results in an larger improvement to the Hubble residuals description.

In the case of the "n-step", we find the global optimal step location to be $n = -0.15$, with a maximum significance of 2.56σ, a magnitude of 0.062 ± 0.024 mag and $\Delta RMS = 0.0027$. In the local case, we find the optimal step location to be $n = -0.475$, with a maximum significance of 1.37σ, a step magnitude of 0.030 ± 0.022 mag and $\Delta RMS = 0.0006$. These are simultaneously the lowest step significance levels, magnitudes and ΔRMS observed for the standard calibration.

Looking at Figs. 2, it is clear that the values obtained for the optimal "dust" and "n-step" locations coincide fairly closely with the median values of τ_V and n close to the optimal "mass-step" locations. For this reason, it is safe to conclude that these steps simply recover the original "mass-step" relation. However, judging from both the significance levels and values of ΔRMS observed for each step, the "mass step" appear to be the preferable way to describe and correct for this effect.

It might be the case, however, that looking for a "τ_V-step" or a "n-step" individually cannot account for the correct division of dust properties between the two SNe Ia populations. Thus, rather than considering only one of these parameters when dividing the two step populations, we will examine what happens when both parameters are simultaneous taken into account. Essentially, we adopt the same formalism used above, with the difference that a two dimensional step location is now considered.

We find the optimal population division to be: one population consisting of SNe Ia with $\tau_V < \tau_{V_{\mathrm{step}}}$ and $n > n_{\mathrm{step}}$ and another consisting of the rest. Under these conditions, for the global case, we find the optimal step location to be $\tau_V = 1.81$ and $n = -0.85$, with a maximum significance of 4.11σ, a magnitude of 0.085 ± 0.020 mag and $\Delta RMS = 0.0068$. For the local case, we find the optimal step location to be $\tau_V = 0.82$ and $n = -0.975$, with a maximum significance of 4.37σ, a step magnitude of 0.091 ± 0.021 mag and $\Delta RMS = 0.0046$.

For the global case, the values obtained for the two dimensional "dust-step" significance, magnitude and

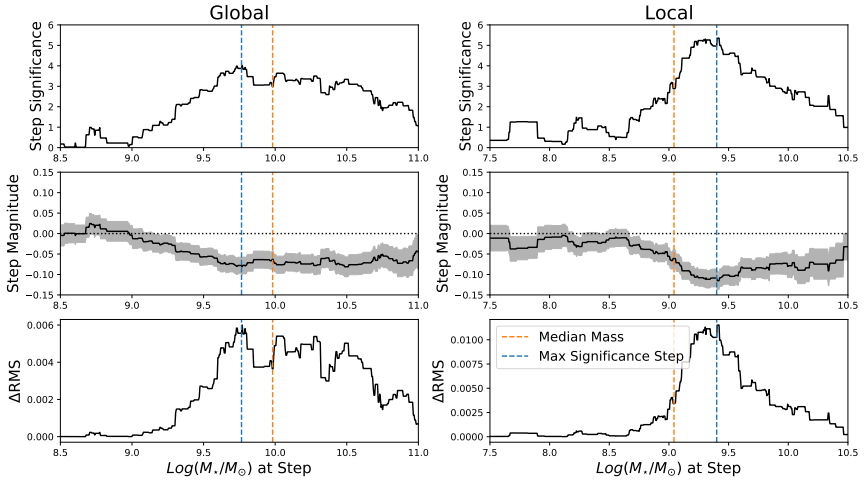

FIG. 4. Evolution of the "mass-step" significance, magnitude and ΔRMS using SNe Ia standard β calibration for the global (Left panels) and local (Right panels) cases. In each case, and for each step location, the top panel shows the significance of the step in σ, the middle panel shows the magnitude of the step in solid black, with the grey region showing the uncertainty, and the lower panel shows the difference between $RMS_{\rm mean}$ and $RMS_{\rm step}$. In these three panels, the location of the step of maximum significance is shown in blue and the median mass of the sample is shown in orange. Based on Kelsey (2020)[11].

ΔRMS are almost identical to those obtained for the original "mass-step". Being able to recover this "mass-step" relation using only host galaxy attenuation parameters is rather enlightening. The results are not as good for the local case, but the two dimensional "dust-step" is still the closest at reproducing the "mass-step".

Although we cannot definitely conclude as to whether or not the "mass-step" has its origin in dust effects, it appears that an attenuation based description for this phenomenon is possible and, under the right conditions, as favourable as the more common mass description.

B. New SNe Ia Calibration

We can now look at the new SNe Ia calibration. The *best-fit* values found for the global R_V case were $\alpha = 0.438^{+0.009}_{-0.011}$, $\beta_{\rm int} = 4.317^{+0.013}_{-0.010}$ and $M = -19.096^{+0.010}_{-0.012}$. Additionally, we obtain $RMS = 0.442$, which represents an increase of 0.305 in relation to the standard calibration. For the local R_V case, the *best-fit* values found were $\alpha = 0.152^{+0.010}_{-0.011}$, $\beta_{\rm int} = 3.099^{+0.009}_{-0.011}$ and $M = -18.775^{+0.010}_{-0.009}$. In addition, we obtain $RMS = 0.622$, which represents an increase of 0.485 in relation to the standard calibration

Overall, judging from the values of RMS, these calibrations appear to be worst fits of the data than the standard calibration, which once again indicates that host attenuation laws do not accurately describe SN extinction. It is particularly surprising that the global measurements result in a smilingly better fit than the local ones.

Examining both calibrations in terms of their Hubble residuals and the possible "mass-step", we find that the results differ greatly from those obtained for the standard calibration. For the global case, the optimal step location is found to be $\mathrm{Log}(M_\star/M_\odot) = 9.22$. This step corresponds to a maximum significance of 2.52σ, a step magnitude of 0.206 ± 0.079 mag and $\Delta RMS = 0.0083$. In the local case, the optimal step is $\mathrm{Log}(M_\star/M_\odot) = 9.02$, with a maximum significance of 3.47σ, a step magnitude of 0.240 ± 0.068 mag and $\Delta RMS = 0.0288$.

While taking the R_V values into account does seem to lower the significance levels of the recovered "mass-steps", this appears to be a consequence of the increased level of scatter in the Hubble residuals, as evidenced by the large step magnitudes. It should be noted, however, that the values of ΔRMS indicate the new calibration ends up strengthening the "mass-step", rather than reducing it. On the whole, it seems that the "mass-step" cannot be fully eliminated by SNe Ia calibration when considering only the attenuation laws for the respective host galaxies. A more in-depth study of the SNe inherent extinction is needed to obtain a truly correct calibration.

VII. CONCLUSIONS

The problem of SNe Ia calibration and the study of astronomical dust remain central to the field of Cosmology. In this work we have explored ways to better probe the dust contents of SNe Ia host galaxies.

We have shown through simulations that DECam *griz* photometry is enough to recover dust properties for simulated SNe Ia host galaxies, provided one employs a well calibrated Bayesian fitting procedure.

We found that, using both global and local DECam

griz photometry, we can recover dust properties for host galaxies that are consistent with literature predictions based on both simulations and observations. We find a relation of the dust attenuation slope with the dust optical depth, both locally and globally, that is best explained with varying star to dust geometry with galaxy orientation. Most importantly, we show that dust properties vary greatly across different galaxies, meaning a universal SNe Ia β correction cannot be assumed.

The relation between both attenuation parameters is found to be very different from the extinction relations obtained directly for SNe Ia, making the comparison between the two somewhat difficult. On one hand, the values of τ_V obtained for the hosts give a good insight into the dust optical depths affecting the respective SNe Ia, as this property is not particularly affected by dust/star geometry. On the other hand, SNe reddening does not seem to be well described by values found for the slope of the host's attenuation laws. This is due to the different phenomena involved in extinction and attenuation.

Shifting our attention to the Hubble residuals resulting from the standard SNe Ia calibration, we conclude that there is some evidence for both individual τ_V and n "steps", even though both of these appear to reflect the same tendency expressed by the "mass-step", although less clearly. However, when using both attenuation parameters to define a two dimensional "dust-step" for the global case, we were able to recover a step with roughly the same significance, magnitude and RMS improvement observed for the "mass-step". This opens the door for a fully attenuation based description of the phenomenon.

Finally, we conclude that an alternative SNe Ia calibration, incorporating the values of R_V and $E(B-V)$ obtained for the host galaxies as an approximation of the extinction of the SNe, results in a worse fit for the SNe. This is mostly attributed to the large differences between host galaxy attenuation and SN Ia extinction, meaning the values for β_{R_V} cannot be correctly determined.

Generally, although the results related to host galaxy attenuation presented in this work constitute an important step forward, their applicability to SNe Ia cosmology is still mostly limited and deserves further study.

[1] A. G. Riess et al., Astronomical Journal **116**, 1009 (1998).
[2] S. Perlmutter et al., Astrophysical Journal, Supplement **517**, 565 (1999).
[3] R. Tripp, Astronomy and Astrophysics **331**, 815 (1998).
[4] M. Sullivan et al., Monthly Notices of the Royal Astronomical Society **406**, 782 (2010).
[5] D. Brout et al., The Astrophysical Journal **874**, 150 (2019).
[6] J. J. Condon and A. M. Matthews, Publications of the Astronomical Society of the Pacific **130**, 073001 (2018).
[7] S. Salim and D. Narayanan, Annual Review of Astronomy and Astrophysics **58**, 529–575 (2020).
[8] S. González-Gaitán et al., Monthly Notices of the Royal Astronomical Society (2021).
[9] S. Salim, M. Boquien, and J. C. Lee, The Astrophysical Journal **859**, 11 (2018).
[10] D. E. S. Collaboration: et al., Monthly Notices of the Royal Astronomical Society **460**, 1270 (2016).
[11] L. Kelsey et al., Monthly Notices of the Royal Astronomical Society **501**, 4861–4876 (2020).
[12] B. Flaugher et al., The Astronomical Journal **150**, 150 (2015).
[13] M. Smith et al., Monthly Notices of the Royal Astronomical Society **494**, 4426 (2020).
[14] P. Wiseman et al., Monthly Notices of the Royal Astronomical Society **495**, 4040–4060 (2020).
[15] Bertin, E. and Arnouts, S., Astron. Astrophys. Suppl. Ser. **117**, 393 (1996).
[16] D. J. Schlegel, D. P. Finkbeiner, and M. Davis, The Astrophysical Journal **500**, 525 (1998).
[17] E. L. Fitzpatrick, Astrophysical Journal, Supplement **299**, 219 (1985).
[18] B. L. and et al., astropy/photutils: v0.6, 2019.
[19] J. Leja, B. D. Johnson, C. Conroy, P. G. v. Dokkum, and N. Byler, The Astrophysical Journal **837**, 170 (2017).
[20] D. Foreman-Mackey, D. W. Hogg, D. Lang, and J. Goodman, Publications of the ASP **125**, 306 (2013).
[21] D. W. Hogg and D. Foreman-Mackey, The Astrophysical Journal Supplement Series **236**, 11 (2018).
[22] G. Bruzual A., Philosophical Transactions of the Royal Society A: Mathematical, Physical and Engineering Sciences **368**, 783 (2010).
[23] P. Marigo and L. Girardi, Astronomy and Astrophysics **469**, 239 (2007).
[24] C. Conroy, J. E. Gunn, and M. White, Astrophysical Journal, Supplement **699**, 486 (2009).
[25] C. Conroy and J. E. Gunn, Astrophysical Journal, Supplement **712**, 833 (2010).
[26] P. Kroupa, Monthly Notices of the RAS **322**, 231 (2001).
[27] E. R. Stanway and J. J. Eldridge, Monthly Notices of the Royal Astronomical Society **479**, 75–93 (2018).
[28] D. Calzetti et al., The Astrophysical Journal **533**, 682–695 (2000).
[29] Noll, S. et al., A&A **507**, 1793 (2009).
[30] M. Kriek and C. Conroy, The Astrophysical Journal **775**, L16 (2013).
[31] C. Erickson, *GauPro: Gaussian Process Fitting*, 2021, R package version 0.2.4.
[32] J. Chevallard, S. Charlot, B. Wandelt, and V. Wild, Monthly Notices of the RAS **432**, 2061 (2013).
[33] D. Narayanan, C. Conroy, R. Davé, B. D. Johnson, and G. Popping, The Astrophysical Journal **869**, 70 (2018).
[34] K. S. Mandel, G. Narayan, and R. P. Kirshner, The Astrophysical Journal **731**, 120 (2011).
[35] D. Brout and D. Scolnic, The Astrophysical Journal **909**, 26 (2021).